Three-dimensional dense distributed temperature sensing for measuring layered thermohaline systems

Hilgersom, Koen; van de Giesen, Nick; de Louw, PGB; Zijlema, Marcel

DOI
10.1002/2016WR019119

Publication date
2016

Document Version
Final published version

Published in
Water Resources Research

Citation (APA)
Hilgersom, K., van de Giesen, N., de Louw, PGB., & Zijlema, M. (2016). Three-dimensional dense distributed temperature sensing for measuring layered thermohaline systems. *Water Resources Research*, *52*(8), 6656–6670. Article WR019119. https://doi.org/10.1002/2016WR019119

AGU PUBLICATIONS

Water Resources Research

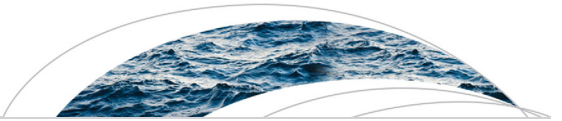

RESEARCH ARTICLE
10.1002/2016WR019119

Key Points:
- A fiber-optic DTS setup was designed to measure detailed temperature profiles in three dimensions
- The setup avoids the application of continuing coils for high-resolution temperature sensing
- Detailed temperature signatures in thermohaline stratified water bodies are captured

Supporting Information:
- Supporting Information S1
- Movie S1
- Movie S2
- Movie S3
- Movie S4

Correspondence to:
K. P. Hilgersom,
k.p.hilgersom@tudelft.nl

Citation:
Hilgersom, K. P., N. C. van de Giesen, P. G. B. de Louw, and M. Zijlema (2016), Three-dimensional dense distributed temperature sensing for measuring layered thermohaline systems, *Water Resour. Res.*, *52*, 6656–6670, doi:10.1002/2016WR019119.

Received 26 APR 2016
Accepted 10 AUG 2016
Accepted article online 16 AUG 2016
Published online 27 AUG 2016

Three-dimensional dense distributed temperature sensing for measuring layered thermohaline systems

K. P. Hilgersom[1], N. C. van de Giesen[1], P. G. B. de Louw[2], and M. Zijlema[3]

[1]Water Resources Section, Faculty of Civil Engineering and Geosciences, Delft University of Technology, Delft, Netherlands, [2]Department of Soil and Groundwater, Deltares, Utrecht, Netherlands, [3]Environmental Fluid Mechanics Section, Faculty of Civil Engineering and Geosciences, Delft University of Technology, Delft, Netherlands

Abstract Distributed temperature sensing has proven a useful technique for geoscientists to obtain spatially distributed temperature data. When studies require high-resolution temperature data in three spatial dimensions, current practices to enhance the spatial resolution do not suffice. For example, double-diffusive phenomena induce sharp and small-scale temperature patterns in water bodies subject to thermohaline gradients. This article presents a novel approach for a 3-D dense distributed temperature sensing setup, the design of which can be customized to the required spatial resolution in each dimension. Temperature is measured along fiber-optic cables that can be arranged as needed. In this case, we built a dense cage of very thin (1.6 mm) cables to ensure that interference with flow patterns was minimal. Application in water bodies with double-diffusion-induced sharp temperature gradients shows that the setup is well able to capture small-scale temperature patterns and even detects small unsuspected seeps and potential salt-fingers. However, the potential effect of the setup on the flow patterns requires further study.

1. Introduction

With the advance of distributed temperature sensing (DTS) in environmental sciences, several studies have applied this technique to monitor vertical high-resolution temperature gradients in a surface water body [*Vercauteren et al.*, 2011; *Suárez et al.*, 2011; *Hausner et al.*, 2012; *Van Emmerik et al.*, 2013]. Wrapping the fiber-optic cable to a coil has proven a useful strategy when only detailed data of the temperature profile in one dimension is of interest. However, when small-scale gradients in multiple dimensions are relevant, this method is less practical, because:

1. Sampling points anywhere on the coil, which usually has a diameter of several centimeters, are integrated to a single point in the horizontal.
2. The fiber-optic cables are often wound around a tube. Locating several tubes closely together significantly disturbs flows in the water column.

The aim of this study is to accurately measure horizontally and vertically varying temperature profiles with DTS. A new DTS setup is designed to measure small-scale 3-D temperature profiles in a surface water body, which overcomes the mentioned disadvantages of wrapped coils. We apply this setup, here called *Dense DTS*, in small-scale thermohaline systems. The setup is largely able to capture the spatial temperature variability caused by double-diffusive processes.

1.1. Distributed Temperature Sensing

Temperature has long been recognized as a suitable tracer for measuring water flows [*Slichter*, 1905]. For example, contrasting temperatures can help characterizing groundwater contributions to a surface water body [*Stonestrom and Constantz*, 2003; *Anderson*, 2005]. Most studies require multiple temperature measurements, for example, to measure temperature gradients [*Euser et al.*, 2014; *Suárez et al.*, 2011; *Steele-Dunne et al.*, 2010]. Since the previous decade, distributed temperature sensing (DTS) has made its way into environmental sciences. This technique allows to measure numerous temperature samples along a fiber-optic cable, offering an efficient and accurate alternative for traditional temperature sensors [*Selker et al.*, 2006a; *Tyler et al.*, 2009].

DTS is based on the principle of scattering of a light signal traveling along an optical fiber. When collapsing on small discontinuities in the glass fiber, part of the photons shift in wavelength. As a consequence, the

light signal that scatters back toward the light source carries temperature information in its wavelength spectrum. Of the five discernible wavelength bands in a backscattered signal, the most common DTS technique in Earth sciences employs the ones with the shortest and longest wavelengths, i.e., the Raman bands. The light intensities in the band with the shortest wavelengths, the anti-Stokes component, is strongly temperature-dependent. The band with the longest wavelengths, the Stokes component, is weakly temperature-dependent. Raman DTS uses the ratios of the light intensities of the Stokes and anti-Stokes components to derive the temperatures along the cable. Accounting for the travel time of the signal up and down the cable allows to assess each sampling location in the fiber-optic cable.

Currently, the Silixa Ultima (Silixa Ltd., London, UK) DTS instrument provides the highest sampling resolution, sampling each 13 cm along the fiber-optic cable. Several studies that required a higher spatial resolution wound the fiber-optic cable to a coil [*Ciocca et al*., 2012; *Euser et al*., 2014]. Many of these studies used PVC tubes as a support for these coils [*Selker et al*., 2006b; *Suárez et al*., 2010a, 2011; *Vogt et al*., 2010, 2012; *Vercauteren et al*., 2011]. *Hilgersom et al*. [2016b] show that wrapping cables to narrow coils and the use of PVC support tubes can have adverse effects on the measurements. Cables with an internal stuffing of the fiber exist [*Arnon et al*., 2014], but do not reach the desired spatial resolution in many applications where detailed measurements are required.

1.2. Thermohaline Stratification

Many studies on thermohaline stratification at the oceanic scale have been published [*Stommel and Fedorov*, 1967; *Stern*, 1967; *Ruddick and Gargett*, 2003; *Kelley et al*., 2003; *Yoshida and Nagashima*, 2003; *Kimura et al*., 2011]. The abundance of such layering in oceans made this research field the main driver of research to double-diffusive processes [*Huppert and Turner*, 1981]. However, more recently, numerous publications appeared on thermal stratification in lakes [*Schmid et al*., 2004; *Arnon et al*., 2014], ponds [*Giestas et al*., 2009; *Suárez et al*., 2010b], and boreholes [*Berthold and Börner*, 2008]. Although a fundamental phenomenon on the molecular scale, many of these studies managed to accurately model stratification at these larger scales.

Systems with vertical temperature and salinity gradients exist in various forms. When the lower part of the water body is more saline and colder, the system is unconditionally stable, and diffusion of heat and salt is the only driver to counter the stratification. Because both gradients act stabilizing, we refer to these systems as *stable*. In the opposite *unstable* case, stratification can never exist and layers tend to overturn by convection, as the more saline and colder water near the surface is always denser than the water below.

So-called double-diffusion occurs in the case of opposing salt and temperature gradients, as long as the bottom layer is denser. In oceans, stratified systems occur with warm and saline water overlaying colder and fresher water. These systems are characterized by *salt fingers* or, in the presence of shear flow, salt sheets [*Kimura et al*., 2011]. The opposite case is more often witnessed in lakes and mineshafts, where colder and fresher water near the surface induces a layered system with *double-diffusive convection* [*Schmid et al*., 2004]. Both for salt fingering and double-diffusive convection, diffusion increases the density gradients between two layers, maintaining its stratification [*Ruddick and Gargett*, 2003].

Larger-scale and stable thermohaline systems allow for accurate monitoring by probing the water body with a single temperature or salinity sensor. In oceans, deep lakes, and boreholes, for example, determining the temperature profile with a frequency of months to years can suffice to analyze how the layers in the system evolve [*Schmid et al*., 2004]. When using multiple point sensors or a distributed sensor, more frequent monitoring is possible [*Arnon et al*., 2014].

Thermohaline stratification is also observed at smaller scales. For example, *De Louw et al*. [2010, 2013] described the inflow of saline preferential groundwater seeps into ditches of deep polder areas (reclaimed lakes), which are situated 4–7 m below mean sea level. These *boils* can reach salinities up to 5 g L^{-1} and are found to be the dominant salinization source in the Dutch deep polders [*De Louw et al*., 2010]. Boils occur as small vents in ditches (pin boils), or as small sand volcanoes (Figure 1).

Boils have a fairly constant temperature throughout the year that is colder than the surface water during summer and warmer during winter. The outflow of saline boil water with a constant temperature induces a stratified system with the relatively freshwater in the ditch on top. Double-diffusive convection occurs when the surface water is colder but less dense than the boil seepage.

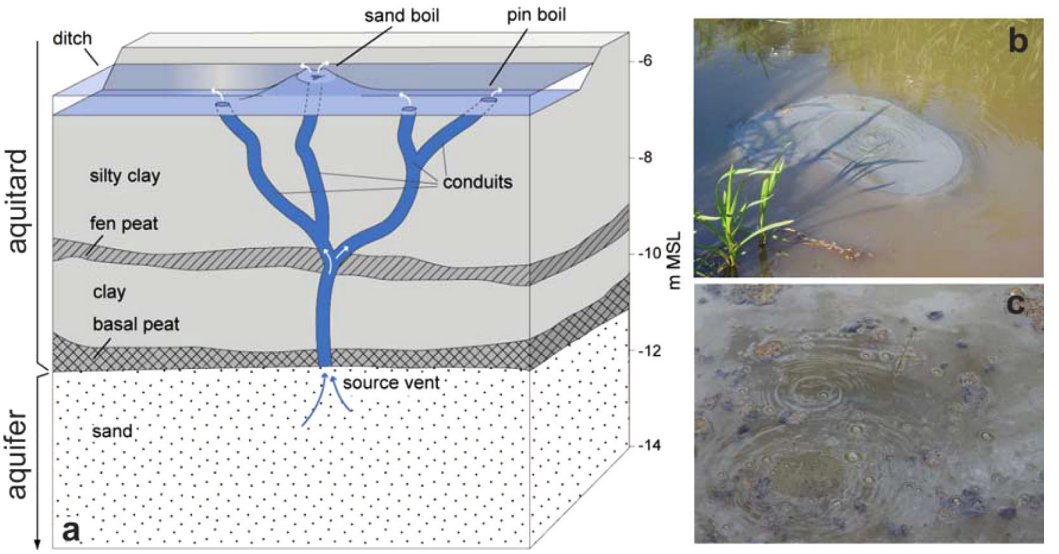

Figure 1. (a) Schematized boil conduits. (b) A sand volcano. (c) Boils sometimes transport methane gas from the subsoil [*De Louw et al.*, 2010].

In this paper, boils are used to investigate the opportunities of Dense DTS for studying layered thermohaline systems where small-scale double-diffusive processes play a role. When coupling the temperature data to a hydrodynamic model, Dense DTS potentially allows to monitor seepage inflows with a contrasting temperature, whereas conventional methods require the placing of heat probes in the streambed [*Naranjo and Turcotte*, 2015; *Stonestrom and Constantz*, 2003]. This article focuses on the ability of Dense DTS to observe the development of, and temperature patterns in these layered systems.

2. Materials and Methods

2.1. Three-Dimensional DTS Setup

In order to accurately measure horizontally and vertically varying temperature profiles, we defined the following criteria for our DTS setup:

1. The setup should be able to accurately monitor horizontally varying temperature patterns.
2. The influence of the setup on the local water flow should be as small as possible.
   Our specific application for sharp thermohaline interfaces imposed an additional criterion.
3. The setup should be able to monitor with a high vertical resolution around the sharp interface, which is located in the bottom third of the setup for the present case studies.

It appeared that a setup with horizontally distributed standing PVC conduits undesirably influences the water flow and does not provide enough opportunity to measure with a very fine vertical resolution. Besides, cables wrapped around small diameter PVC tubes can negatively influence the measurements [*Hilgersom et al.*, 2016b]. We therefore chose for a setup in which horizontal nets of fiber-optic cable are spanned across a cage. In this way, closely spanned layers can provide sufficient temperature data near the sharp interface and the only material influencing the flow is the thin fiber-optic cable that occupies a maximum of 2% of the setup volume for the closely spaced cable nets.

The cage, with outer dimensions of 1 m $\times$ 1 m $\times$ 1 m, consists of 80 vertical bars with a helical groove to embed the fiber-optic cable at each turnaround. The bars are 25 mm PVC conduits, which are kept in place by three PVC squares, the bottom and top ones being 12 mm thick and the middle one being 8 mm thick (Figure 2). At each turnaround, the cable is fixed in the groove with white duct tape, which inhibits shifting of the cable. The white color is chosen to prevent undesired heating of the setup due to solar irradiation [*Hilgersom et al.*, 2016b].

In our setup, we used two tight-buffered, bend proof 1.6 mm multimode cables (AFL, part number SR0015161001) with lengths of 1143 and 1243 m. The only strain protection in the cables consisted of

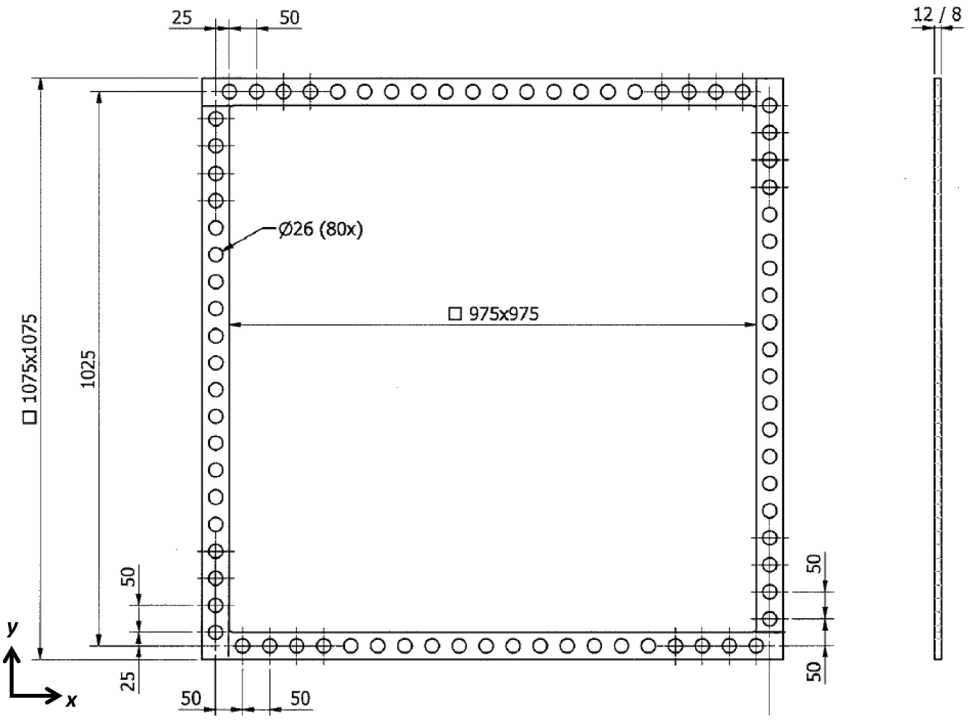

Figure 2. Size (in millimeters) of the PVC rings with the locations of the mounting holes for the PVC conduits.

aramid fibers. Based on lab experiments (unpublished), we concluded that the signal attenuation is still low enough for accurate measurements at a bend diameter as small as 25 mm. The employed Ultima-S DTS device (Silixa Ltd., London, UK) has a sampling interval of 13 cm and a spatial resolution of about 25–30 cm. This resolution is necessary to measure horizontally varying temperature patterns with the described setup. The two cables connect to the DTS device at both ends, and each of the four channels successively uses a 30 s integration time per time interval. For these settings, the manufacturer reports a temperature resolution of approximately 0.05°C. To display a complete temperature profile for a certain point in time, the more than 34,000 data samples within the cage are linearly interpolated over time.

DTS machines employ a calibration strategy to convert Raman scattered photon signals from all along the fiber-optic cable into temperatures. *Hausner et al*. [2011] and *Van de Giesen et al*. [2012] showed that manual calibration of the temperature measurements using the raw Stokes and anti-Stokes data usually outperforms the standard machine calibration. Besides, the bends in our setup might cause spatially varying differential attenuation [*Hilgersom et al*., 2016b]. We therefore applied the manual double-ended calibration presented in *Van de Giesen et al*. [2012]. Another advantage of manual calibration is that we can get a better grip on the data and spot possible flaws introduced by the many cable bends in the setup.

Van de Giesen et al. [2012] described the manual calibration procedure for the differential attenuation, the energy shift between a photon at the incident wavelength and a scattered photon (γ), and the time-varying calibration parameter $C(t)$. We chose to calibrate differential attenuation and values for γ per cable and values for $C(t)$ per individual measurement direction. These parameters are used to calculate the temperature at each individual sampling point from the locally measured Stokes and anti-Stokes signal.

The locations of the sampling points in the setup are determined by placing the setup in an outside environment of approximately 2°C, and filling three PVC tubes at each corner with hot water. Based on the local temperature peaks, the center of each turnaround at the PVC tubes can be determined with an estimated accuracy of $\sim$0.03 m. Applying this procedure to data collected in both directions along the cable further increases the accuracy. The position of the cables at the corner points consequently is then known in the *xyz*-grid used for locating all the sampling points within the cage. The other turnaround positions follow from division of the cable distance in-between the corner locations over the amount of spans for each layer. The grid locations of the sampling points are then calculated for each span individually.

The tight-buffered cables tend to expand and shrink significantly with changing environmental temperatures. We therefore expanded the calibration procedure with an additional length correction to better determine the location dependent calibration parameters, and to determine the varying locations of the temperature samples during the measurements. During the calibration procedure, the cable length was determined for each point in time by applying a linear expansion coefficient to the cable-averaged machine calibrated temperatures.

The linear expansion coefficient is cable-specific, and was derived from differences in average cable length between the measurement periods. The cable lengths were determined first by matching temperature samples recorded from both ends of each cable. Based on the cable lengths and average temperatures during three case studies (section 2.3) and during the determination of the sampling point locations (approximately 2°C), the linear expansion coefficient of the cable was found to be 2.6×10^{-5} K^{-1}, with a standard deviation of 3.5%. This is in accordance with the linear expansion coefficients of other glass fiber reinforced polymers.

2.2. Thermohaline Stratification

To determine whether the thermohaline systems in our case studies are stable, unstable, or promote double-diffusive layering, the Turner angles, *Tu*, of these systems are calculated [*Ruddick*, 1983]:

$$Tu = arctan\left(\frac{N_T^2 - N_S^2}{N_T^2 + N_S^2}\right), \tag{1}$$

where $N_T^2 = -g\alpha\partial T/\partial z$, $N_S^2 = g\beta\partial S/\partial z$, T is the temperature, S is the salinity, and the z axis is in downward direction. A stable system occurs for $|Tu| < 45°$, whereas $|Tu| > 90°$ yields a gravitationally unstable system. Double-diffusive convection occurs for $-90° < Tu < -45°$, and salt fingering for $45° < Tu < 90°$.

The thermal expansion coefficient, α, and solutal expansion coefficient, β, are dependent on temperature and salinity itself, and are calculated for the average salinity and temperature on the interface. We employ coefficients derived from a linear regression to the density derivatives to temperature and salinity, where the density is calculated from an approximation to the UNESCO formula [*UNESCO*, 1981] by *Wright* [1997]:

$$\alpha(T,S) = -2.285097\times10^{-5} + 1.324876\times10^{-5}\cdot T - 9.288537\times10^{-8}\cdot T^2 + 1.563353\times10^{-6}\cdot S, \tag{2}$$

$$\beta(T,S) = 7.998742\times10^{-4} - 2.774404\times10^{-6}\cdot T + 3.188185\times10^{-8}\cdot T^2 - 4.151510\times10^{-7}\cdot S. \tag{3}$$

2.3. Case Studies

This paper presents results from laboratory measurements (Case 1), and field measurements in the surface water covering boils in the Noordplas Polder (Case 2) and Kortenhoef (Case 3), all in the Netherlands. The complete data sets and additional graphical representations are published in *Hilgersom et al.* [2016a].

2.3.1. Case 1: Laboratory Measurements

The laboratory setup consisted of a 2.5 m × 2.5 m container, containing water up to a level of 0.5 m with a salinity ranging from 0.7 to 1.4 g L^{-1} (Figure 3). In this study, we slowly built up a more saline layer from below. The water, with a salinity ranging from 2.6 to 2.9 g L^{-1}, entered the container through a circular hole with a diameter of 0.5 m located in the center of the bottom. The hole was covered with an antirooting membrane to equally distribute the inflowing water over the hole. The water level was maintained by placing vertical pipes, which were pinched over the full depth, in the four corners of the container. Siphons lead the water in the pipes outside the container into buckets, which were filled to their top edge located at the water level, and in total were overflowing with the same discharge as the inflow.

The actual purpose of this setup was to simulate saline boil seepage inflow, but it also provides the opportunity to study a layered thermohaline system. The inflow salinities and temperatures were monitored with a CTD-diver (Schlumberger Water Services, Delft, the Netherlands) underneath the antirooting membrane. As a reference, the temperatures near the bottom and near the water surface were monitored with two TD-divers (Schlumberger Water Services, Delft, the Netherlands).

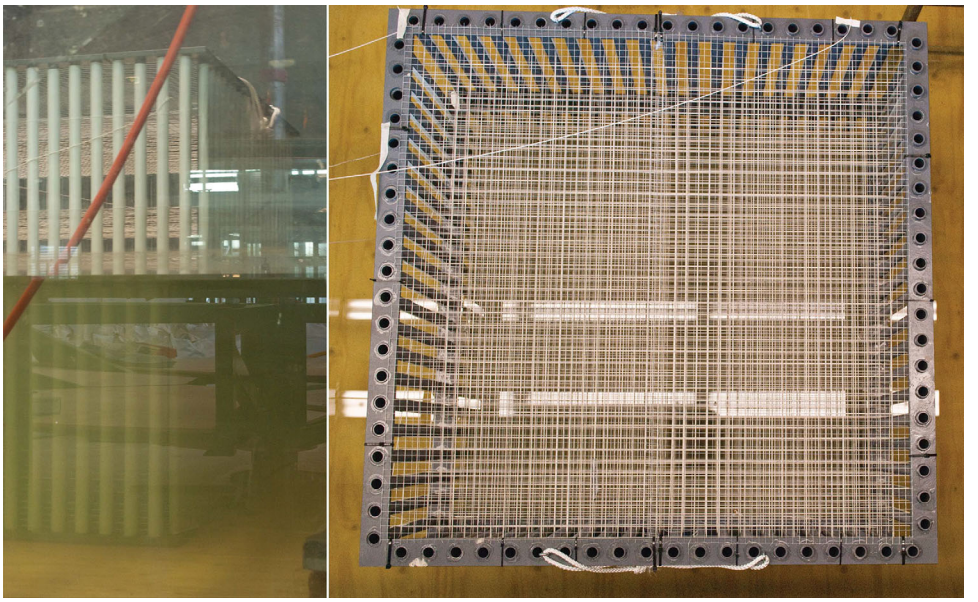

Figure 3. DTS setup deployed in a laboratory test setup.

Table 1 divides the laboratory measurements into six runs, all performed between 19 August and 21 August 2013. Salinities were calculated from measured electrical conductivities normalized to a reference temperature of 25°C according to the equation presented by *Schemel* [2001]. The inflowing water had a higher salinity, and a temperature that was either higher or lower than the surface water temperature. The surface water was mixed before each run in order to prevent initial variations in temperature and salinity. Based on the Turner angles, we expected that stable layering developed when cold water flowed in from the bottom, and double-diffusive convection when warm water flowed in. The conduits in the laboratory setup delayed the inflow of water with the desired properties, causing time-varying inflow discharges (Q), salinities (S), and temperatures (T). Therefore, the presented inflow properties are averages.

2.3.2. Case 2: Field Measurements Noordplas Polder

During earlier studies, saline boils were observed in the Noordplas Polder [*De Louw et al.*, 2013; *Vandenbohede et al.*, 2014; *Hut et al.*, 2016]. The inflow of highly saline water through the bottom of a relatively freshwater body is expected to cause a stratified system with freshwater above saline water. Also during winter, the warmer saline water has a higher density than the colder freshwater in the ditch, causing double-diffusive convection ($-69° < Tu < -45°$ for the measured salt gradient between groundwater and surface water).

The DTS setup was placed at the bottom of the ditch above a boil in the Noordplas Polder from 28 September until 11 October 2013. In this paper, we focus on the part of the measurement period between 9 October and 11 October, when outside temperatures dropped from several degrees Celsius above toward several degrees Celsius below the boil temperature. To check the occurrence of stratification, the salinities and temperatures near the bottom and near the water surface were monitored with two CTD-divers.

Table 1. Water Temperatures (T) and Salinities (S) of the Surface Water and the Inflow, and Inflow Discharges (Q), for the Six Runs[a]

		Surface Water		Inflow			Stability	
Run	Duration (h)	T (°C)	S (g L^{-1})	Q (m^3 h^{-1})	T (°C)	S (g L^{-1})	Nature	Tu (°)
1	2.4	22.3	0.7	0.11	**25.9**	2.6	DDC	−82.2
2	2.2	22.6	0.9	0.10	**25.8**	2.4	DDC	−89.3
3	4.8	22.8	1.0	0.11	**27.2**	2.5	DDC	−85.8
4	3.4	**22.8**	1.2	0.11	21.8	2.6	STA	−30.0
5	1.9	22.7	1.35	0.12	**25.1**	2.9	DDC	−85.7
6	3.6	**22.8**	1.4	0.13	21.5	2.7	STA	−23.1

[a]Bold temperatures indicate the highest values (surface water versus inflow). The last two columns indicate the physical stability of the layered system based on Turner angle Tu: unconditionally stable (STA) or double-diffusive convection (DDC).

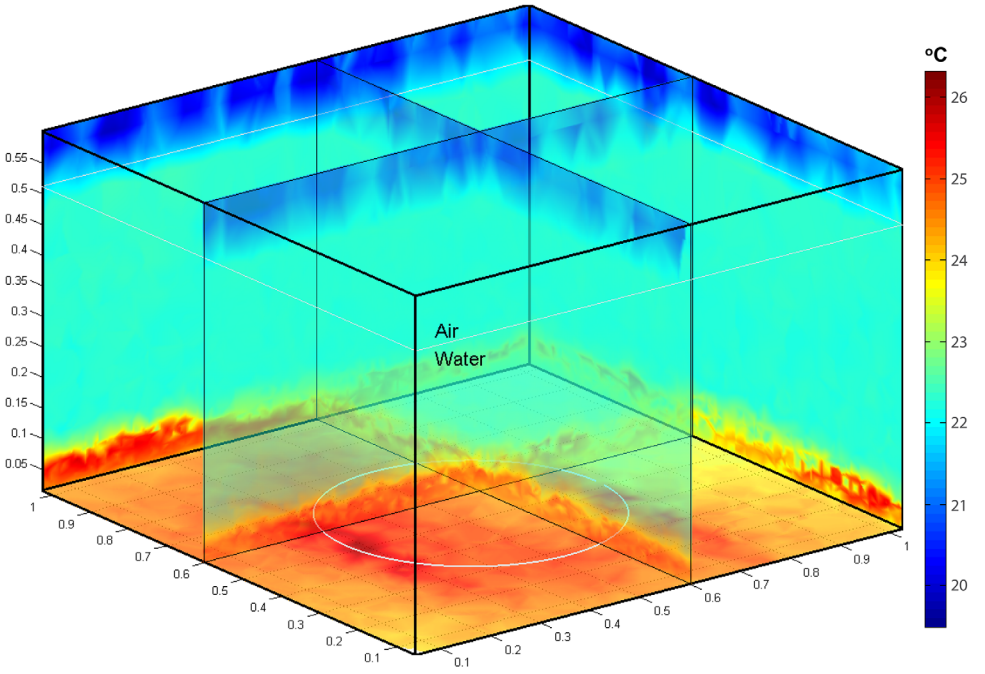

Figure 4. Three-dimensional representation of a measured temperature profile in the laboratory setup.

We increased the water level to about 14 cm in order to stimulate the development of a layered system by building a small weir downstream. This weir was placed far enough not to influence the development of a saline layer around the boil, but close enough to decrease circulating currents as a consequence of a large wind fetch over the ditch. The discharge over the weir was measured several times during the field campaign by recording the time required to fill a bucket, and varied between 0.3 and 0.7 L s^{-1}. These discharges yielded a negligible flow velocity of maximum 5 mm s^{-1} through the ditch of about 1 m wide. This was confirmed by acoustic flow measurements with an OTT ADC (OTT Hydromet, Loveland, CO, USA), which reported similar values with a maximum of 15 mm s^{-1}. The flow velocity from boils in the Noordplas can reach values up to 10 mm s^{-1} [*De Louw et al.*, 2010].

2.3.3. Case 3: Field Measurements Kortenhoef

At the measurement site in Kortenhoef, boils discharging freshwater occur. Presumably, this preferentially exfiltrating groundwater was infiltrated in a nearby ice-pushed ridge. The surface water in this system is slightly more saline (measured salinities between 0.22 and 0.29 g L^{-1}) due to seepage inflows of shallower groundwater. In this case, the thermohaline system is expected to produce salt fingers when the temperature in the surface water is more than 0.5°C higher than the boil seepage temperature ($45° < Tu < 90°$), and else to be unstable.

Between 17 and 24 March 2014, the DTS setup monitored the surface water temperature above a freshwater boil with a salinity of 0.17 g L^{-1}. The water level was controlled manually by a downstream gate and was on average 22 cm; due to a sloping bed, 18 cm on the right side and 27 cm on the left side of the setup viewing downstream. OTT ADC measurements reported a maximum flow velocity of 0.03 m s^{-1} at the water surface. However, most of the time the flow velocities reduced to almost 0 m s^{-1}. As in Case 2, CTD divers monitored temperatures and salinities near the bottom and water surface.

3. Results and Discussion

3.1. Case 1: Laboratory Measurements

This subsection presents results from two laboratory simulations with different temperature and salinity contrasts (Table 1). Figure 4 presents an example of a 3-D temperature profile obtained by our measurement setup. The supporting information (movies S1 to S4) displays the time evolution of the 3-D temperature profiles for the measurements presented in this article. The DTS setup measured with a decreasing

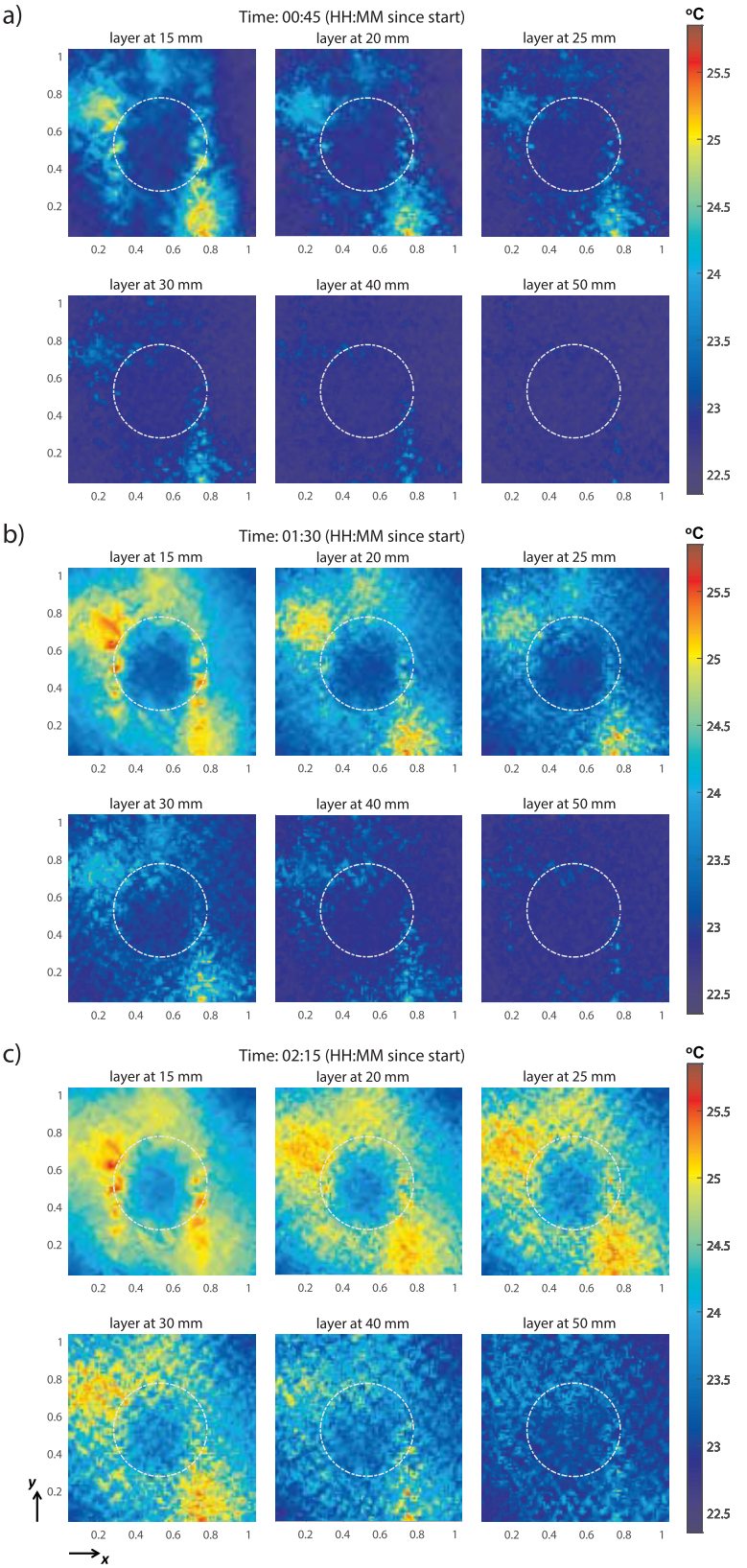

Figure 5. Horizontal temperature slices for a hot inflow in the laboratory setup (Run 2), at 15, 20, 25, 30, 40, and 50 mm above the bed. The displayed situations are at (a) 0h45, (b) 1h30, and (c) 2h15 after the start of the measurements.

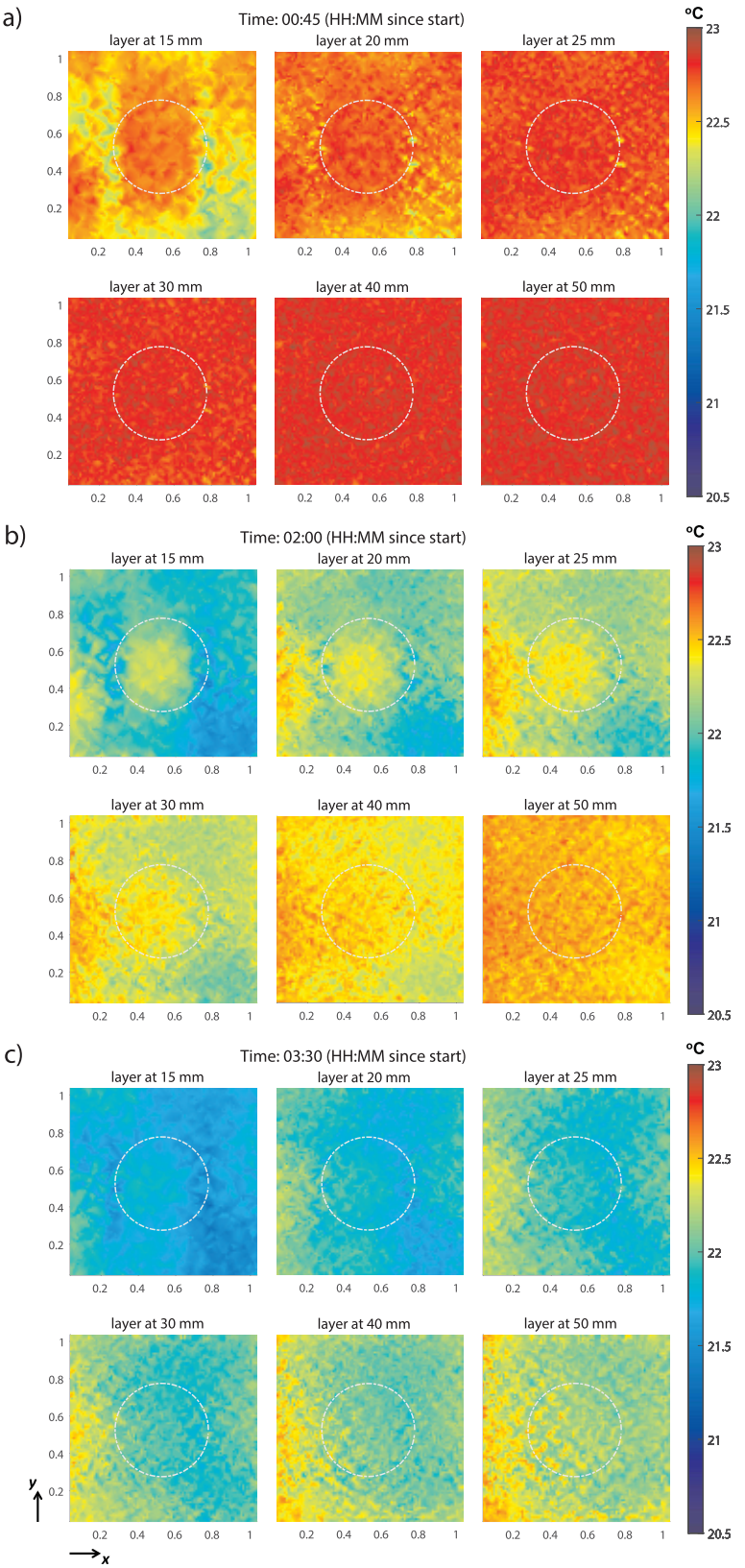

Figure 6. Horizontal temperature slices for a cold inflow in the laboratory setup (Run 6), at 15, 20, 25, 30, 40, and 50 mm above the bed. The displayed situations are at (a) 0h45, (b) 2h00, and (c) 3h30 after the start of the measurements.

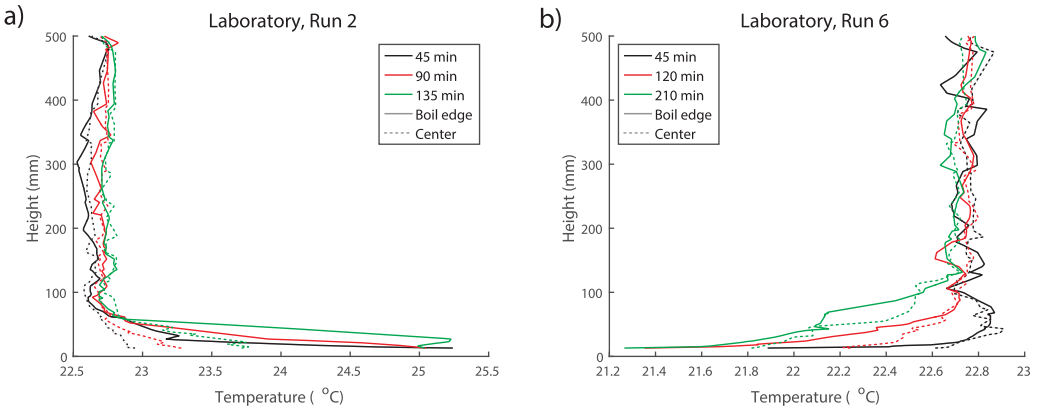

Figure 7. Vertical temperature profiles for two case studies in the laboratory. The locations are selected to mark the differences between the temperature profiles above the boil center and the boil edge.

vertical resolution toward the top. As a consequence, the temperatures near the air-water interface appear noisy after linear interpolation over space. However, here we are only interested in detailed measurements in the lower part of the water column.

To allow a more detailed analysis, we show results of Runs 2 and 6 (Figures 5 and 6, respectively) as horizontal slices at six different levels, and at different moments. This way, one can see the interface evolve. In both simulations, the higher slices uniformly show the initial temperatures 45 min after the measurements have started (Figures 5a and 6a). At this time, the lower slices already show locations where the seepage water disturbs the interface.

Although the seepage water is expected to rise vertically through the covered circular hole, the disturbed interfaces in both cases show a square pattern around the inflow location (Figures 5 and 6). Apparently, the antirooting membrane was less permeable than expected, causing the water to seep sideways. The square pattern of warm upflowing water matches the location of the wooden strips used to nail the membrane to the floor. This can be considered a defect of the laboratory setup. However, at the same time, it demonstrates the DTS setup capability to locate such temperature patterns with centimeter accuracy.

For Run 2, we observe that on the locations where water is seeping sideways from the inflow, it consequently flows upward over the bottom 4 cm (Figure 5). Based on the Turner angle (Table 1), it is expected that local convection cells are formed as the most effective physical mechanism to counteract the temperature and salt gradient between the inflowing water and the surface water (i.e., double-diffusive convection). Although the occurrence of convection cells cannot be concluded from the data, we observe the tendency of diffusing heat in lateral and upward direction from the light blue colors surrounding the yellow patterns in Figure 5.

At the latest stage of Run 2 (Figures 5c and 7a), a clear interface is developing at about 50 mm, with the warmer water more spread over the bottom layer. This is the moment that the water body starts to clearly develop toward a dual-layered system that is not much disturbed by the inflow properties. At about 50 mm, one can see that the interface is still not completely homogeneous. This could be the remainder of the disturbance caused by the inflow. Alternatively, the inhomogeneities in the interface, which exceed the temperature resolution of the measurements ($\sim$0.05°C), can be caused by the cables themselves. Their influence is expected to be small, since their relative volume over the complete setup is only 0.4%, and in the bottom 10 cm it is 2%, but the cable nets could induce small-scale convection cells by the physical tendency to diffuse the temperature interface.

For Run 6, the inflowing colder and fresher water promotes the development of a stable interface. The lack of a buoyancy-inducing gradient yields molecular diffusion as the main physical driver to counteract the salt-temperature interface. Again, we observe the initial inflow disturbances, extending to about 30 mm (Figures 6a and 6b). After more than 2 h, the cold lower layer starts to become more homogeneous over the horizontal cross section (Figure 6c). At the interface, though, again some inhomogeneities are visible that could be caused by the cable nets themselves. The effect of the cable nets is difficult to quantify, and

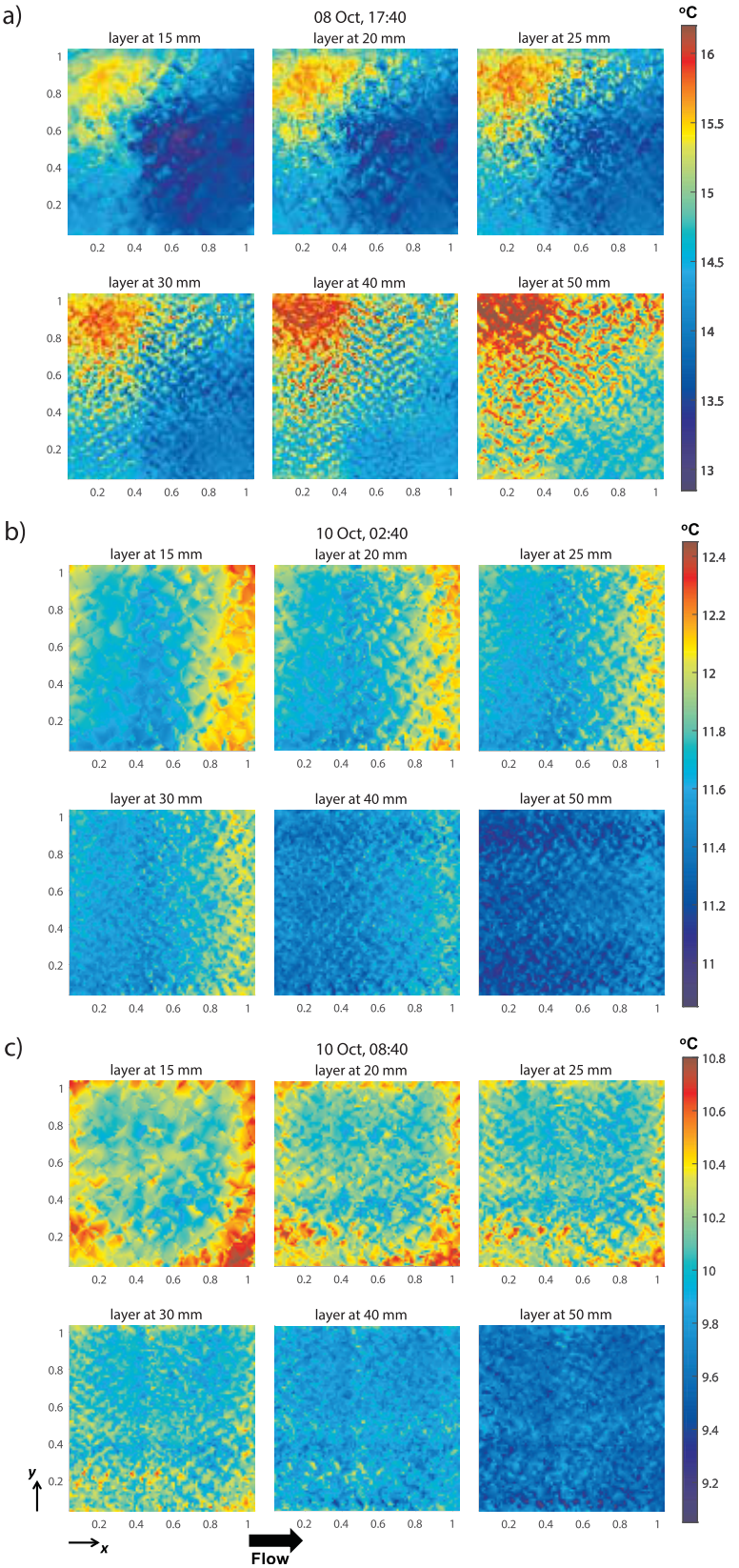

Figure 8. Horizontal temperature slices at 15, 20, 25, 30, 40, and 50 mm above a boil seep in the Noordplas Polder. The displayed situations are during (a) a warm afternoon (8 October 2013, 17:40), (b) at the start of a cold night after a warm day (10 October 2013, 2:40), and (c) at the end of a cold night after a warm day (10 October 2013, 8:40).

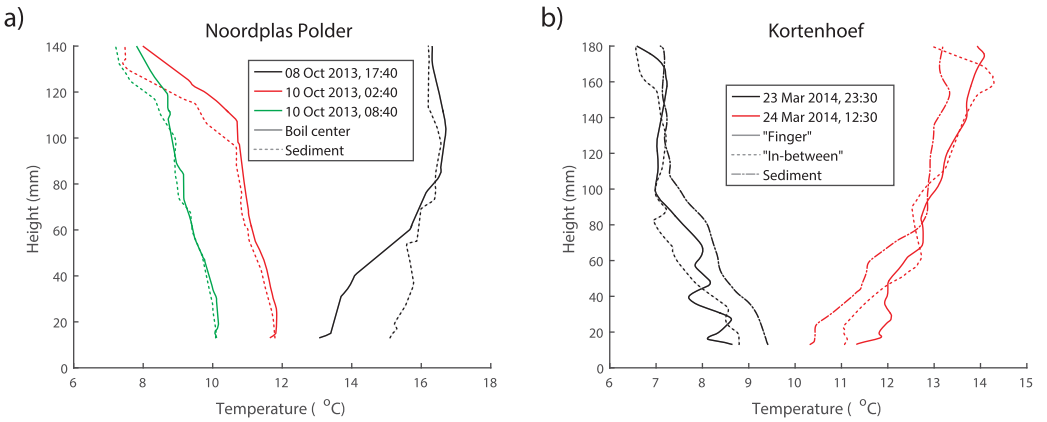

Figure 9. Vertical temperature profiles for the case studies in the Noordplas Polder (a) and Kortenhoef (b). The locations of the temperature profiles are selected to mark interesting differences in the vertical temperature patterns.

we recommend further study on how it affects the flow patterns. Figure 7b displays a delayed rise of the interface above the boil compared to the interface at the boil edge throughout the measurement period.

3.2. Case 2: Field Measurements Noordplas Polder

The measurement campaign in the Noordplas Polder comprised a transition from a warmer period to a colder period. This, together with the diurnal temperature fluctuation, allows us to compare a warm surface water situation (Figure 8a) with a situation where the surface water is turning cold (Figures 8b and 8c).

During the warm period, the cold and saline seepage water builds up a stable interface above the boil ($|Tu| < 45°$). A diffusive layer, between 40 and 60 mm, forms an interface between the seepage and surface water layer (Figure 9a). The hot top left corner of Figure 8a marks a local sediment deposit up to a level of 50 mm, which was formed over the previous days and was under direct forcing of solar radiation. Due to high upward velocities, boils often transport sand from the aquifer to the surface, as illustrated by the sand volcano in Figure 1b. The lower rim of the DTS setup apparently changed the flow profile near the bottom allowing local sediment settlement. Around the sediment deposit, the colder seepage water spread over the bottom in the other directions.

During the transition period, the surface water started to cool down from the top. Underneath, a warm layer temporarily persisted, which was disrupted by the slightly less warm seepage water in the center of our measurement setup (Figure 8b). The hot spots near the edges of Figure 8b show that sediment, which was heated over the past day, had further accumulated around the boil during the measurement period. Due to the salinity gradient, both the seepage water and the surrounding warm water remained denser than the overlying surface water ($-69° < Tu < -45°$). The weak diffusive layering at these Turner angles is not clearly visible in Figure 9a, although some unsharp steps can already be spotted for the small temperature gradient at this time. On October 10, 2:40, the surface water has cooled down to about 11.2°C at a level of 50 mm. The sediment temperature is approximately 1°C higher.

At 8:40, the sediment has further cooled down to 10.7°C, and the cold water has reached the lower 1.5 cm (Figure 8c). In the center, the warmer seepage water mixes with the surface water within the lower 30 mm, above which the temperature decreases stepwise (Figure 9a).

3.3. Case 3: Field Measurements Kortenhoef

Like Case 2, the field data from Kortenhoef show accumulation of sediment around the boil. Particularly during night, the heat sustaining sediment show clear temperature patterns (Figure 10a). Although the seepage water is approximately 10°C, no direct traces of it are visible, as it tends to mix directly with the surface water. A colder horizontal band is visible around $y \approx 0.25$ m, which is on the shallow side of the DTS setup.

At 12:30 the next day, the sediment shows a delayed heating of 1°C compared to the enclosed surface water near the bottom (Figure 10b). This time a warmer horizontal band is visible on the shallow side. Interestingly, a diffusive interface has developed at 50 mm above the bottom, from which salt fingers seem to

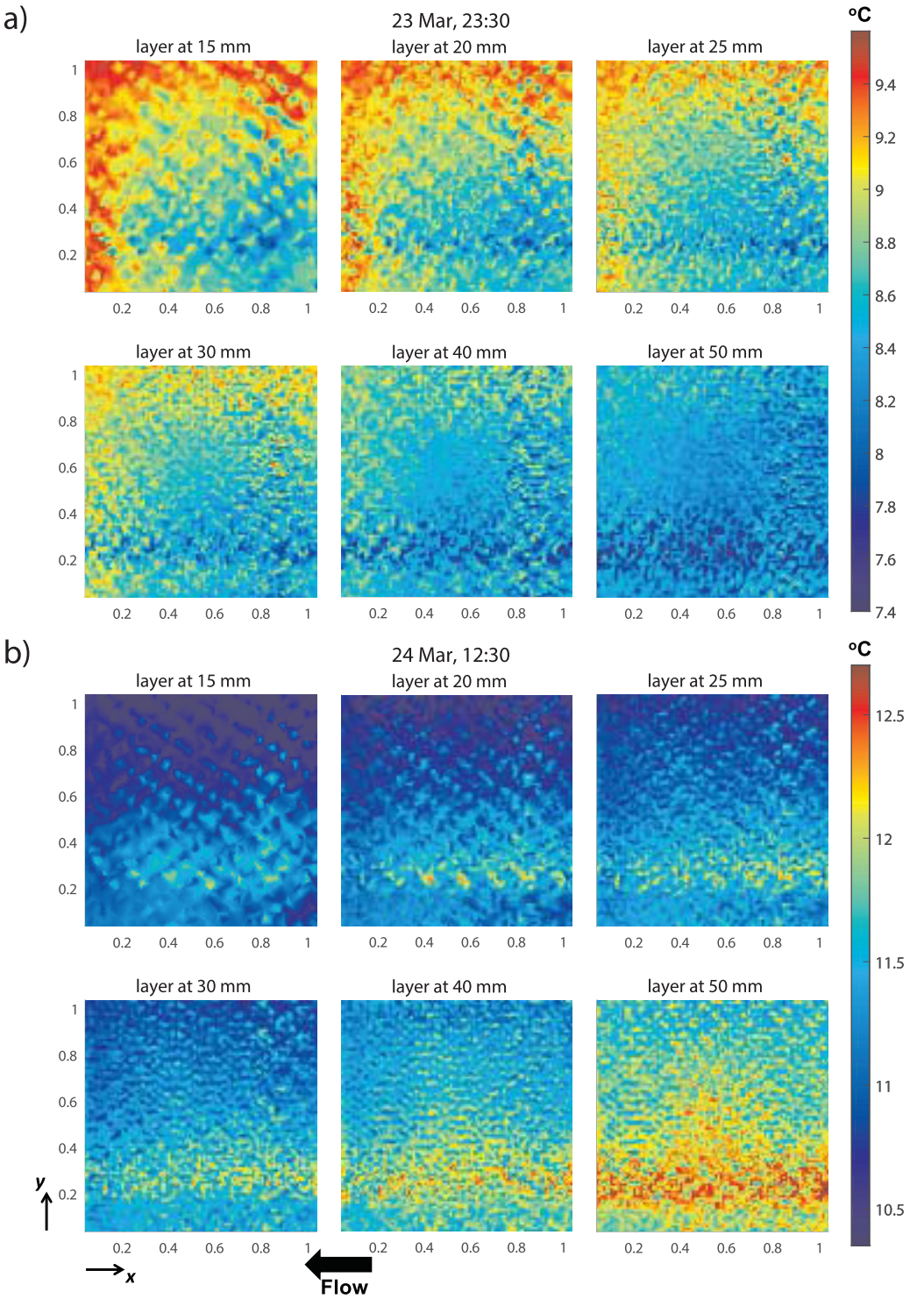

Figure 10. Horizontal temperature slices at 15, 20, 25, 30, 40, and 50 mm above a boil seep in Kortenhoef. The displayed situations are during (a) a cold night after a warm day (23 March 2014, 23:30) and (b) a warm afternoon (24 March 2014, 12:30).

develop. The temperature patterns of the downward salt fingers extend to the layer at 15 mm, where they are still visible as yellow dots. In the layers above, these yellow dots widen, while approximately sustaining their position, although the data shows some interference patterns for the highest layers. Figure 9b plots the temperature profiles at the location of an assumed salt finger and at a location in between two salt

fingers. The salt finger temperature is up to 1°C higher underneath the interface at 50 mm, and colder above. Despite this clear pattern, care should be taken, as the temperature patterns at these two locations also differed at night, when overturning of the less dense bottom layer was expected.

The occurrence of weak salt fingering is expected based on the salinity gradient and a temperature gradient of more than 0.5°C (section 2.3). The data show that the DTS setup was able to potentially localize these small-scale patterns.

4. Conclusion

This article describes a new DTS setup which allows 3-D high-resolution temperature measurements. Stacked layers of cables woven through a cage in two horizontal directions allow the acquisition of a 3-D grid of temperature data points with free-to-choose resolutions. Because of our interest in thermal processes near the streambed, we have chosen a very high vertical resolution within the lower 10 cm. Although the cable is bent at each turnaround, continuous coils are prevented. In order to correctly calibrate the temperature measurements and the location of the cable, the calibration method by *Van de Giesen et al*. [2012] was expanded with a procedure to account for thermal expansion of the cable.

One of the purposes of the 3-D DTS setup is to study the evolution of temperature patterns in detail. Temperature measurements in three case studies demonstrated the setup capability to observe small-scale temperature patterns, such as local seeps and double-diffusive processes. Although we have to be careful in our conclusions for the occurrence of salt fingers in Case 3, theory from double-diffusive phenomena confirm that they potentially occur in the studied thermohaline system. Besides, the accumulation of sediment around the studied boil seeps in lowland areas (Cases 2 and 3) could be observed based on the sediment's delayed heating and cooling compared to the surface water.

The influence of the DTS setup on the observed water systems is difficult to quantify. In the laboratory studies, the closely spaced cable nets seemed to slightly influence the development of thermohaline interfaces. These disturbances need to be studied in more detail to be conclusive about the influence of the measurement setup. However, the absence of cable supports in the area of interest makes it unlikely that the setup influences the measurements more than the currently used constructions for coil-wrapped DTS (e.g., PVC conduits).

We recommend further study of the performance of the DTS setup for small-scale patterns, as caused by salt fingers, in a laboratory setup. This can for example be done by improving the presented laboratory setup with a uniform inflow, allowing to slowly build up an interface with warmer and more saline water on top. Variation of the environmental temperature could allow to further study temperature effects on the calibrated cable positioning within the device.

Acknowledgments

This project is funded by Netherlands Organisation for Scientific Research (NWO) project 842.00.004. Further, we would like to thank Tim van Emmerik, Wouter Berghuijs, and Marlies Barendrecht for their dedicated help in designing and building the DTS setup, Mr. Dorrepaal (Noordplas) and Miss Schneider (Kortenhoef) for hosting our field measurements, and Rob Tijsen (Waternet) for making us aware of the fresh boils in Kortenhoef. The data set can be accessed online (doi:10.4121/uuid:da1d236b-7d0a-4c67-9136-bf913a7aa1b2 [*Hilgersom et al*., 2016a]). The supporting information (movies S1 to S4) presents alternative representations of the laboratory and field data.

References

Anderson, M. P. (2005), Heat as a ground water tracer, *Ground Water*, *43*(6), 951–968.

Arnon, A., N. G. Lensky, and J. S. Selker (2014), High-resolution temperature sensing in the dead sea using fiber optics, *Water Resour. Res.*, *50*, 1756–1772, doi:10.1002/2013WR014935.

Berthold, S., and F. Börner (2008), Detection of free vertical convection and double-diffusion in groundwater monitoring wells with geophysical borehole measurements, *Environ. Geol.*, *54*, 1547–1566, doi:10.1007/s00254-007-0936-y.

Ciocca, F., I. Lunati, N. Van de Giesen, and M. B. Parlange (2012), Heated optical fiber for distributed soil-moisture measurements: A lysimeter experiment, *Vadose Zone J.*, *11*(4), 9851 pp.

De Louw, P., G. Oude Essink, P. Stuyfzand, and S. van der Zee (2010), Upward groundwater flow in boils as the dominant mechanism of salinization in deep polders, the Netherlands, *J. Hydrol.*, *394*, 494–506, doi:10.1016/j.jhydrol.2010.10.009.

De Louw, P., A. Vandenbohede, A. Werner, and G. O. Essink (2013), Natural saltwater upconing by preferential groundwater discharge through boils, *J. Hydrol.*, *490*, 74–87, doi:10.1016/j.jhydrol.2013.03.025.

Euser, T., W. M. J. Luxemburg, C. S. Everson, M. G. Mengistu, A. D. Clulow, and W. G. M. Bastiaanssen (2014), A new method to measure Bowen ratios using high-resolution vertical dry and wet bulb temperature profiles, *Hydrol. Earth Syst. Sci.*, *18*(6), 2021–2032, doi:10.5194/hess-18-2021-2014.

Giestas, M., H. L. Pina, J. P. Milhazes, and C. Tavares (2009), Solar pond modeling with density and viscosity dependent on temperature and salinity, *Int. J. Heat Mass Transfer*, *52*, 2849–2857, doi:10.1016/j.ijheatmasstransfer.2009.01.003.

Hausner, M., F. Suárez, K. Glander, N. Giesen, J. Selker, and S. Tyler (2011), Calibrating single-ended fiber-optic Raman spectra distributed temperature sensing data, *Sensors*, *11*(11), 10,859–10,879.

Hausner, M. B., K. P. Wilson, D. B. Gaines, and S. W. Tyler (2012), Interpreting seasonal convective mixing in devils hole, death valley national park, from temperature profiles observed by fiber-optic distributed temperature sensing, *Water Resour. Res.*, *48*, W05513, doi:10.1029/2011WR010972.

Hilgersom, K., N. van de Giesen, P. de Louw, and M. Zijlema (2016a), 3D dense DTS: Temperature data from waterbodies subject to thermohaline stratification—Laboratory measurements and field campaigns in the Noordplas Polder and at Kortenhoef, TU Delft, Netherlands, doi:10.4121/uuid:da1d236b-7d0a-4c67-9136-bf913a7aa1b2.

Hilgersom, K., T. van Emmerik, A. Solcerova, W. Berghuijs, J. Selker, and N. van de Giesen (2016b), Practical considerations for enhanced-resolution coil-wrapped distributed temperature sensing, *Geosci. Instrum. Methods Data Syst.*, *5*(1), 151–162, doi:10.5194/gi-5-151-2016.

Huppert, H. E., and J. Turner (1981), Double-diffusive convection, *J. Fluid Mech.*, *106*, 299–329.

Hut, R., S. Tyler, and T. van Emmerik (2016), Proof of concept: Temperature-sensing waders for environmental sciences, *Geosci. Instrum. Methods Data Syst.*, *5*(1), 45–51, doi:10.5194/gi-5-45-2016.

Kelley, D. E., H. J. S. Fernando, A. E. Gargett, J. Tanny, and E. Özsoy (2003), The diffusive regime of double-diffusive convection, *Prog. Oceanogr.*, *56*(3–4), 461–481, doi:10.1016/S0079-6611(03)00026-0.

Kimura, S., W. Smyth, and E. Kunze (2011), Turbulence in a sheared, salt-fingering-favorable environment: Anisotropy and effective diffusivities, *J. Phys. Oceanogr.*, *41*(6), 1144–1159.

Naranjo, R. C., and R. Turcotte (2015), A new temperature profiling probe for investigating groundwater-surface water interaction, *Water Resour. Res.*, *51*, 7790–7797, doi:10.1002/2015WR017574.

Ruddick, B. (1983), A practical indicator of the stability of the water column to double-diffusive activity, *Deep Sea Res., Part I*, *30*, 1105–1107.

Ruddick, B., and A. E. Gargett (2003), Oceanic double-infusion: Introduction, *Prog. Oceanogr.*, *56*(3–4), 381–393, doi:10.1016/S0079-6611(03)00024-7.

Schemel, L. (2001), Simplified conversions between specific conductance and salinity units for use with data from monitoring stations, *IEP Newsl.*, *14*(1), 17–18.

Schmid, M., A. Lorke, C. Dinkel, G. Tanyileke, and A. Wüest (2004), Double-diffusive convection in lake Nyos, Cameroon, *Deep Sea Res., Part I*, *51*(8), 1097–1111, doi:10.1016/j.dsr.2004.02.010.

Selker, J., N. van de Giesen, M. Westhoff, W. Luxemburg, and M. Parlange (2006a), Fiber optics opens window on stream dynamics, *Geophys. Res. Lett*, *33*, L24401, doi:10.1029/2006GL027979.

Selker, J., L. Thévenaz, H. Huwald, A. Mallet, W. Luxemburg, N. van de Giesen, M. Stejskal, J. Zeman, M. Westhoff, and M. Parlange (2006b), Distributed fiber optic temperature sensing for hydrologic systems, *Water Resour. Res*, *42*, W12202, doi:10.1029/2006WR005326.

Slichter, C. (1905), Field measurements of the rate of movement of underground waters, *U.S. Geol. Surv. Water Supply Pap.*, *140*, 1–122.

Steele-Dunne, S., M. Rutten, D. Krzeminska, M. Hausner, S. Tyler, J. Selker, T. Bogaard, and N. van de Giesen (2010), Feasibility of soil moisture estimation using passive distributed temperature sensing, *Water Resour. Res.*, *46*, W03534, doi:10.1029/2009WR008272.

Stern, M. E. (1967), Lateral mixing of water masses, *Deep Sea Res. Oceanogr. Abstr.*, *14*(6), 747–753, doi:10.1016/S0011-7471(67)80011-1.

Stommel, H., and K. Fedorov (1967), Small scale structure in temperature and salinity near Timor and Mindanao, *Tellus, Ser. A*, *19*(2), 306–325.

Stonestrom, D., and J. Constantz (2003), Heat as a tool for studying the movement of ground water near streams, *U.S. Geol. Surv. Circ., 1260*, 1–96.

Suárez, F., A. Childress, and S. Tyler (2010a), Temperature evolution of an experimental salt-gradient solar pond, *J. Water Clim. Change*, *1*(4), 246–250.

Suárez, F., S. Tyler, and A. Childress (2010b), A fully coupled, transient double-diffusive convective model for salt-gradient solar ponds, *Int. J. Heat Mass Transfer*, *53*(9–10), 1718–1730, doi:10.1016/j.ijheatmasstransfer.2010.01.017.

Suárez, F., J. Aravena, M. Hausner, A. Childress, and S. Tyler (2011), Assessment of a vertical high-resolution distributed-temperature-sensing system in a shallow thermohaline environment, *Hydrol. Earth Syst. Sci.*, *15*(3), 1081–1093, doi:10.5194/hess-15-1081-2011.

Tyler, S., J. Selker, M. Hausner, C. Hatch, T. Torgersen, C. Thodal, and S. Schladow (2009), Environmental temperature sensing using Raman spectra DTS fiber-optic methods, *Water Resour. Res*, *45*, W00D23, doi:10.1029/2008WR007052.

UNESCO (1981), Tenth report of the joint panel on oceanographic tables and standards, *UNESCO Tech. Pap. Mar. Sci.*, *36*, 25.

Van de Giesen, N., S. Steele-Dunne, J. Jansen, O. Hoes, M. Hausner, S. Tyler, and J. Selker (2012), Double-ended calibration of fiber-optic Raman spectra distributed temperature sensing data, *Sensors*, *12*(5), 5471–5485.

Vandenbohede, A., P. de Louw, and P. Doornenbal (2014), Characterizing preferential groundwater discharge through boils using temperature, *J. Hydrol.*, *510*, 372–384, doi:10.1016/j.jhydrol.2014.01.006.

Van Emmerik, T., A. Rimmer, Y. Lechinsky, K. Wenker, S. Nussboim, and N. van de Giesen (2013), Measuring heat balance residual at lake surface using distributed temperature sensing, *Limnol. Oceanogr. Methods*, *11*, 79–90.

Vercauteren, N., H. Huwald, E. Bou-Zeid, J. S. Selker, U. Lemmin, M. B. Parlange, and I. Lunati (2011), Evolution of superficial lake water temperature profile under diurnal radiative forcing, *Water Resour. Res.*, *47*, W09522, doi:10.1029/2011WR010529.

Vogt, T., P. Schneider, L. Hahn-Woernle, and O. Cirpka (2010), Estimation of seepage rates in a losing stream by means of fiber-optic high-resolution vertical temperature profiling, *J. Hydrol.*, *380*, 154–164.

Vogt, T., M. Schirmer, and O. A. Cirpka (2012), Investigating riparian groundwater flow close to a losing river using diurnal temperature oscillations at high vertical resolution, *Hydrol. Earth Syst. Sci.*, *16*(2), 473–487, doi:10.5194/hess-16-473-2012.

Wright, D. G. (1997), An equation of state for use in ocean models: Eckart's formula revisited, *J. Atmos. Oceanic Technol.*, *14*(3), 735–740, doi:10.1175/1520-0426(1997)014<0735:AEOSFU>2.0.CO;2.

Yoshida, J., and H. Nagashima (2003), Numerical experiments on salt-finger convection, *Prog. Oceanogr.*, *56*(3–4), 435–459, doi:10.1016/S0079-6611(03)00032-6.